Intermetallics xxx (2009) 1–7

Contents lists available at ScienceDirect

Intermetallics

journal homepage: www.elsevier.com/locate/intermet

Dislocation dynamics simulations of precipitation hardening in Ni-based superalloys with high γ′ volume fraction

A. Vattré [a,*], B. Devincre [b], A. Roos [a]

[a] DMSM, ONERA, 29 Avenue de la Division Leclerc, BP 72, 92322 Châtillon Cedex, France
[b] LEM, CNRS-ONERA, 29 Avenue de la Division Leclerc, BP 72, 92322 Châtillon Cedex, France

ARTICLE INFO

Article history:
Received 27 January 2009
Received in revised form
27 March 2009
Accepted 16 April 2009
Available online xxx

Keywords:
A. Intermetallics, miscellaneous
B. Plastic deformation mechanisms
B. Yield stress
D. Defects: dislocation geometry and arrangement
E. Ordering energies

ABSTRACT

The flow stress of Nickel-based γ/γ′ superalloys containing up to 73 vol.% of Ni_3Al precipitates is calculated by dislocation dynamics simulations of a dislocation pair gliding on {111} planes, for temperatures up to 1000 K. It is calculated for different composition-related parameters (friction stress and APB energy), as well as for different microstructural parameters (channel width, precipitate volume fraction and the geometry of the intersection of the {111} glide plane with the precipitate). The emphasis is on the bowing-assisted cutting regime, which is the prevalent deformation mechanism observed in the simulations.

1. Introduction

Nickel-based γ/γ′ superalloys are extensively used in applications requiring high strength and fatigue resistance up to elevated temperatures, for instance in turbine blades and discs in turbo-engines, and, more recently, in power plants as well. They mainly consist of two phases: a ductile disordered fcc Ni matrix (the γ phase) and coherent $L1_2$-ordered precipitates (the γ′ phase). These precipitates are regularly distributed in roughly cuboidal shapes, with faces parallel to the {100} planes [1]. Unlike normal metals, the yield stress of the intermetallic Ni_3Al-based precipitates exhibits an anomalous temperature dependence [2], and much of the general progress in engine performance derives from the fact that this anomaly persists up to high temperatures. Thus, the trend in Nickel-based superalloy development has been towards increasing the γ′ volume fraction up to values providing an optimum of mechanical properties: the first generation Nickel-based superalloys, such as Waspalloy, contains about 25 vol.% of the γ′ phase, whereas more recently developed alloys may contain up to 70 vol.%.

The interaction between dislocation and precipitates is a classical case where the determination of plastic flow cannot always be evaluated by simple superposition rules. This problem appears to be critical when investigating hardening in γ/γ′ superalloys. Recently, Mohles et al. [3,4,5] have performed numerous two-dimensional dislocation dynamics (DD) simulations in which one or few dislocations glide in a plane intersected by many coherent precipitates, but at a low volume fraction. In addition, Rao et al. [6,7] have carried out DD simulations on γ/γ′ superalloys with up to 40 vol.% of coherent precipitates. In the later work, special attention was paid to the low-temperature yield stress of a Nickel-based superalloy in the cutting regime of small precipitates. In order to extend the work of Rao et al. [6], DD investigations are carried out here for predicting the critical resolved shear stress (CRSS) in the range of high volume fractions, between 40% and 70%. The purpose of the present investigation is twofold. In the first place, we set up and evaluate ingredients for future massive (i.e. with high dislocation densities) three-dimensional DD simulations of γ/γ′ superalloys. Moreover, valuable design guidelines for the development of superalloys and for determining the influence of the microstructural parameters on the mechanical properties can be obtained by these simple computer experiments.

2. Strengthening mechanisms and computer simulations

Plastic yield in superalloys is controlled by the motion of dislocations in the γ matrix channels and their interactions with γ′

* Corresponding author.
E-mail address: aurelien.vattre@onera.fr (A. Vattré).

0966-9795/$ – see front matter © 2009 Elsevier Ltd. All rights reserved.
doi:10.1016/j.intermet.2009.04.007

precipitates and other dislocations. In precipitation-hardened alloys, dislocation–precipitate interactions include Orowan looping and precipitate cutting. In Ni-based superalloys with high precipitate volume fraction, both mechanisms are observed under different deformations or microstructural conditions. From the classical review paper of Pollock and Argon [8], the initial microstructure contains dislocations in the γ matrix, whereas the γ' precipitates are free of dislocations. Upon mechanical loading, dislocations first move through the γ channels, thereby pressing segments of dislocations against the γ/γ' interfaces.

In the γ channels, dislocation motion is hindered by the interactions with solute atoms. The corresponding chemical force has been calculated from post mortem and *in-situ* transmission electron microscopy data on single phase crystals by Saada and Douin [9]. At room temperature it was estimated to correspond to a friction stress of the order of 100 MPa. In the DD simulations here, this solid-solution friction stress is taken into account through a stress τ_{SS} opposing the dislocation motion and this is considered as the elementary mechanism controlling the CRSS of the single γ phase.

The cutting of coherent intermetallic γ' precipitates is controlled by glide of $\langle 110 \rangle$ superdislocations. Such superdislocations are pairs of $1/2(\langle 110 \rangle)$ dislocations (a leading dislocation $D1$ and a trailing dislocation $D2$) with a Burgers vector of magnitude $b = 0.26$ nm. Dislocations $D1$ and $D2$ delimit an antiphase boundary (APB) several nanometers wide [10]. When the leading $1/2(\langle 110 \rangle)$ dislocation glides through the γ' phase, it destroys the $L1_2$ order in the glide plane, thus creating an APB [11]. The subsequent trailing dislocation moving on the same glide plane restores the initial $L1_2$ structure. The APB of energy density γ^{APB} created behind the first dislocation exerts a drag stress $\tau_{APB} = -\gamma^{APB}/b$ on it. This is sufficiently strong to stop the dislocation from penetrating any further into the coherent precipitate. The opposite is true for a second trailing dislocation ($\tau_{APB} = +\gamma^{APB}/b$), i.e. it can enter into the precipitate at lower applied stress.

The $L1_2$ alloys exhibit an anomalous temperature dependence on the flow stress. Takeuchi and Kuramoto [13,14] first proposed that such a yield stress anomaly observed experimentally for Ni_3Ga could be induced by cross-slip from octahedral {111} glide planes onto the cubic {010} planes of screw character dislocations, the Kear–Wilsdorf (KW) locking [1,12]. Subsequently, their model was revised by Paidar et al. [15] for Ni_3Al. Currently, a variety of microstructural models is available for the positive temperature dependence of the flow stress anomaly in $L1_2$ alloys [10]. KW locking is often assumed to take place in the superalloy precipitates, even though this is still the subject of some debates. Recently, Demura et al. [16] revisited this problem and they proposed a simple formulation accounting for the dynamics of dislocation multiplication and immobilization by KW locks. In the latter process, the entire segment cross-slips in one thermal activation event, and thus the activation enthalpy for the KW locking event is a function of the screw segment length. This model provides a simple framework to reproduce the positive temperature dependence of the flow stress and is therefore adopted in the present paper.

The local simulation rules employed in the simulation to account for the formation and destruction of KW locks are duplicated from previous work on Ni_3Al plasticity by Devincre et al. [17,18]. Only the expression for the KW unlocking stress τ_{KW} has been changed in order to be consistent with the Demura et al. model:

$$\tau_{KW} = \sqrt{\mu B f_D \frac{b}{l_S}} \exp\left(-\frac{\Delta H_0}{2kT}\right) \tag{1}$$

with μ the shear modulus (GPa), B a damping constant for dislocation glide (Pa s), k the Boltzmann constant (8.67 eV K^{-1}), f_D a Debye frequency factor (1×10^{13} s^{-1}), l_S the screw segment length (m), T the temperature (K) and ΔH_0 (eV) the activation enthalpy for KW locks (see for details [16,17,18]).

The movement of each dislocation segment is controlled through an effective shear stress τ_{eff} which originates from several different contributions:

- a applied resolved an applied stress τ_{app} accounting for the mechanical loading,
- a solid-solution friction stress τ_{SS},
- a KW unlocking stress τ_{KW},
- a configuration stress τ_{APB} accounting for APB creation or recovery,
- an internal stress τ_{int} accounting for the elastic dislocation–dislocation interactions,
- a line tension term Γ imposed by the discretisation of the line curvature.

For each dislocation segment, its free glide velocity v during one simulation step is determined from

$$v = \begin{cases} 0 & \text{if } \tau_{eff} < \tau_F \\ \dfrac{(\tau_{eff} - \tau_F \mathrm{sign}(\tau_{eff}))b}{B} & \text{if } \tau_{eff} > \tau_F \end{cases} \tag{2}$$

where B is set to 1×10^{-4} Pa s and τ_F a constant friction stress defined by $\tau_F = \tau_{SS}$ in the γ phase, and $\tau_F = \tau_{KW}$ in the γ' phase. The effective stress is given by

$$\tau_{eff} = \tau_{app} + \tau_{int} + \tau_{APB} + \frac{\Gamma}{r}, \tag{3}$$

where r is the local radius of curvature of the dislocation line. Note that $\tau_{SS} = 0$ inside the precipitate and $\tau_{KW} = \tau_{APB} = 0$ in the matrix channels.

The simulated volume is shown in Fig. 1. It contains one γ' cubic precipitate of edge length l surrounded by thin γ channels of width w. The edge length of the simulated volume equals $w + l$ and the volume fraction of precipitate is denoted f. The different geometries of the simulated volumes used in this study are listed in Table 1.

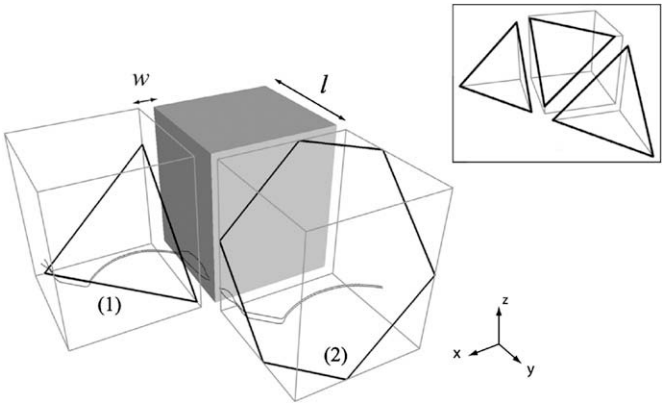

Fig. 1. Drawing of the cubic simulation cell with one γ' precipitate (dark grey) and two replicas illustrating the symmetries imposed by periodic boundary conditions: w is the width of the γ channels, l is the cube edge length of precipitates, and $w + l$ is the edge length of the simulated cell. The two types of superdislocation (111) slip planes considered in this study are shown, respectively an equilateral triangular intersecting plane (1), and a hexagonal intersecting plane (2). As shown in the inset, neighbouring triangular intersections alternatively point up or down.

Please cite this article in press as: Vattré A, et al., Dislocation dynamics simulations of precipitation hardening in Ni-based superalloys with..., Intermetallics (2009), doi:10.1016/j.intermet.2009.04.007

Table 1
Geometrical characteristics as defined in Fig. 1 for the different simulated volumes, and the resulting CRSS for $\gamma^{APB} = 320\ mJ\ m^{-2}$ and $\tau_{SS} = 107$ MPa.

w (μm)	l (μm)	$w+l$ (μm)	f (%)	CRSS (MPa)
0.065	0.580	0.645	73	326
0.065	0.330	0.395	58	266
0.065	0.200	0.265	42	211
0.115	1.050	1.165	73	282
0.115	0.580	0.695	58	225
0.115	0.350	0.465	42	173
0.170	1.550	1.720	73	219
0.170	0.850	1.020	58	167
0.170	0.510	0.680	42	121

In addition, the following simplifying hypotheses are adopted in both phases: the elasticity is isotropic with shear modulus $\mu = 51$ GPa and Poisson ratio $\nu = 0.37$, both at room temperature. Also, only simple glide is considered without cross-slip or climb. All simulations were carried out at room temperature, except those presented in Section 3.6 where the temperature dependence of the flow stress is specifically investigated. All simulations have been performed in a quasi-static regime in which dislocations are pushed slowly against the γ' precipitate. Dislocation lines are discretised into segments with a maximum discretisation length of $w/5$.

Lastly, the DD simulations use periodic boundary conditions to mimic the behavior of a bulk material sample. Such conditions satisfy mechanical equilibrium and provide useful solutions to the problem of dislocation flux balance and line continuity at the boundaries of the simulated volume [19]. In Fig. 1, it can be observed that with such boundary conditions, gliding dislocations can shear the precipitate microstructure either in planes containing a regular periodic pattern of two equilateral triangle interfaces (which are alternatively pointing up and down as shown in the inset of Fig. 1) or in planes containing a regular periodic pattern of hexagonal interfaces. A novel localisation procedure was introduced in the simulations for determining which dislocation segments are candidates for entering pairwise into the precipitate, and whether they are part of a leading or of a trailing dislocation. This is determined by a test on the internal stress τ_{int} at the location of segments entering into the precipitate. Indeed, with only the sign and the amplitude of τ_{int}, one can simply differentiate the cases of leading and trailing dislocations. Details on this procedure will be published in a forthcoming technical paper.

3. Results

For simplicity, γ' precipitates are supposed to be perfectly cubic and the γ/γ' interface is considered as perfectly coherent. The only glide system considered is $\langle 110\rangle\{111\}$. Hence, the intersections between a precipitate and the glide plane of dislocations are triangles or irregular hexagons. At the start of a simulation, one pair of dislocations of either screw or mixed character is placed on a glide plane of one γ channel. Dislocations of mixed type are oriented at an angle of 60° with respect to $\vec{b}$. Due to the periodic boundary conditions, these dislocations are infinitely long and cut an infinite periodic network of precipitates.

For each temperature and for each γ' volume fraction, it was first established that a single dislocation of screw or mixed character could not shear the precipitate network. Such a dislocation can only move around the precipitates, through the γ channels. In this process, the dislocation line is strongly bowed out in the matrix channels, causing a very high Orowan critical stress, which is inversely proportional to the channel width.

Snapshots of a simulation of a 60° dislocation pair cutting though the precipitates are shown in Fig. 2. The stress–strain curve shows a stress drop, which is characteristic of a bowing-assisted cutting process. Such a process can be decomposed into four stages. In Stage 1, the pair of dislocations $D1$ and $D2$ glide into the γ channels. $D1$ is pushed by $D2$ and enters the precipitate at its corners but is then stopped by the process of APB formation. Without trailing dislocation, $D1$ can only enter the γ' precipitate at corners as a result of the strong locally imposed line tension. In Stage 2, assisted by the short-range mutual interaction between $D1$ and $D2$, the resolved shear stress reaches a critical value where the superdislocation is formed and starts entering the precipitates. Sections of $D1$ start to be strongly bowed out in the matrix channels. From this point on, the progression of the superdislocation in the precipitate is mostly controlled by τ_{KW}. In Stage 3, the superdislocation progressively enters the precipitate, but some sections of $D2$ are still anchored at the γ/γ' interface. Finally, in Stage 4, the bowing of $D1$ and $D2$ into the matrix channel drags the superdislocation along, thereby cutting through the whole γ' precipitate.

In this process, strengthening depends on two kinds of parameters. Some parameters are related to the material composition (the APB energy γ^{APB} and the solid-solution friction stress τ_{SS}), the other parameters are related to the material microstructure (the channel width w and the precipitate volume fraction f). In the following sections, the influence of each of these parameters is determined by means of many DD simulations.

3.1. Influence of the APB energy

Fig. 3 shows the CRSS needed by the 60° dislocation pair to overcome the precipitates as a function of γ^{APB}, the APB energy, for a constant channel width $w = 65$ nm and for three different precipitate volume fractions $f = 0.42$, 0.58 and 0.73. Based on literature data, the APB energy is assumed to lie between 100 and 350 mJ m^{-2} [9].

In all simulations, the dislocations overcome the precipitate by bowing-assisted cutting in a strongly coupled regime. For each tested APB energy ($\gamma^{APB} = 100$, 170, 230 and 320 mJ m^{-2}), precipitates were cut by the formation of a superdislocation and its subsequent dragging by dislocations bowing out in the matrix channels. Fig. 3 shows a roughly square root dependence on the APB energy for all three volume fractions. This result is in good agreement with the predictions of Reppich [20]. In the strongly coupled regime, the stress required to cut precipitates increases with the square root of APB energy (as in the present case), whereas in the weakly coupled regime, i.e. when precipitates are cut with one dislocation, the dependence of the cutting stress on APB energy is linear. It is worth noting that the present results are also in agreement with Rao et al. [6] in the case of their largest precipitate size (see [6] Fig. 2 and the 400 nm precipitate edge length).

3.2. Influence of the width of the γ channels

Fig. 4 gives the critical stress required to overcome the precipitates as a function of the channel width $w = 65$, 115 or 170 nm, for a pair of 60° dislocations, a volume fraction $f = 0.73$ and $\gamma^{APB} = 100$, 170, 230 and 320 mJ m^{-2}. Here, the size of the simulated {111} octahedral plane depends on the width w of the channel, with larger simulation cells for larger channel widths. As before, bowing-assisted cutting of the precipitates is observed in all simulations. From Fig. 4 it can be observed that the CRSS is sensitive to the channel width over the whole range of APB energies. The CRSS required to overcome the precipitate is always monotonically decreasing with increasing channel width. Thus, for precipitation hardening in high γ' volume fraction superalloys, a size effect

Please cite this article in press as: Vattré A, et al., Dislocation dynamics simulations of precipitation hardening in Ni-based superalloys with..., Intermetallics (2009), doi:10.1016/j.intermet.2009.04.007

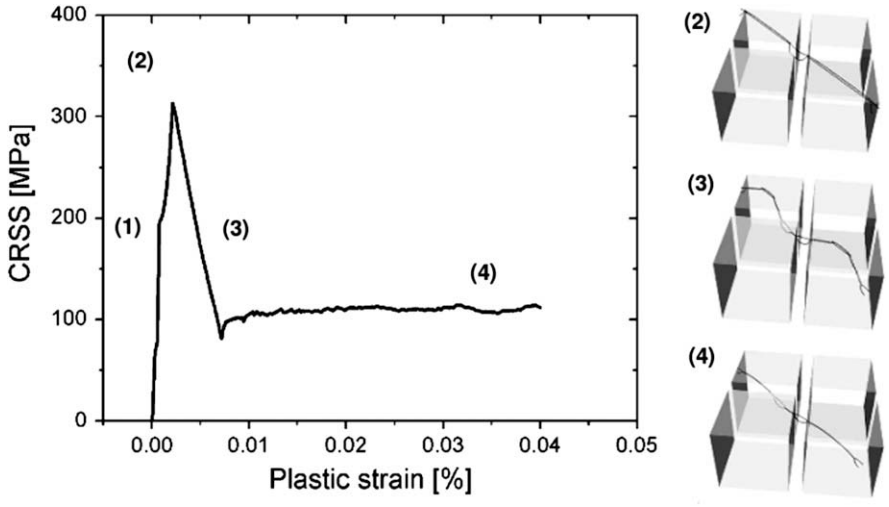

Fig. 2. The four stages of the bowing-assisted cutting process of precipitates. These stages are identified on the simulated stress–plastic strain curve and with the help of snapshots taken from the simulations. In stage (1), plastic deformation only occurs in the matrix channels. In stage (2), the superdislocation starts entering the precipitate. During stage (3), the superdislocation shears the precipitate but sections of the lines remain in the initial γ channels. Stage (4) corresponds to complete shearing of both γ channel and γ' precipitate with a fully formed superdislocation in the latter.

appears in the process of bowing-assisted cutting, but this effect is linearly rather than inversely proportional to w, as theoretically predicted [20,21].

3.3. Influence of the volume fraction of the γ' precipitate

Fig. 5 gives the critical stress required to overcome precipitates as a function of the volume fraction f, for a pair of 60° dislocations. The channel width w was kept constant at 65 nm. As before, the APB energy is increased from 100 to 320 mJ m^{-2} and the volume fraction f of the precipitates was varied from 0.42 to 0.73. Fig. 5 shows that the CRSS increases strongly with increasing volume fraction f when the mean precipitate spacing w is kept constant.

More precisely, in all simulated cases it is observed that the precipitates are cut in the strongly correlated regime. A superdislocation is first formed at the corners of the precipitates and is pulled by the connected pair of dislocations bowing out in the matrix channels. Hence, a higher volume fraction of precipitates at constant channel width is equivalent to increasing the mechanical work to be done by the pulling dislocations in the γ channels. As illustrated in Fig. 5, the CRSS increases linearly with f. This is because a constant length of dislocation in the γ channels pulls an increasing length of superdislocation in the precipitates. Again, the present result is in good agreement with the calculations of Rao et al. [6] at smaller volume fractions of the γ' precipitate, i.e. both lines in Fig. 5 have the same slope. The difference in vertical offset is thought to be caused by the different treatment of the coherency strain: in the present work this is not taken into account, whereas Rao et al. [6] carried out their simulations considering a 0.3% coherency strain.

3.4. Influence of the geometry of the planes cutting the γ' precipitates

Octahedral slip planes intersect cuboidal precipitates in two different ways. As illustrated in Fig. 1, the intersections are either equilateral triangles or irregular hexagons. Fig. 6 compares the

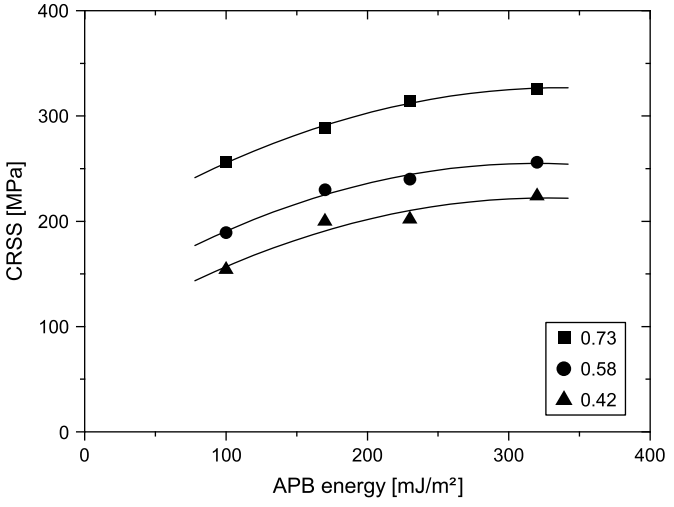

Fig. 3. Results from DD simulations (symbols) of the CRSS for a 60° 1/2⟨110⟩ dislocation pair as a function of APB energy in a superalloy with channel width $w = 65$ nm and with three different volume fractions of precipitates ($f = 0.42$, 0.58, 0.73). The continuous lines fit a square root dependence on APB energy.

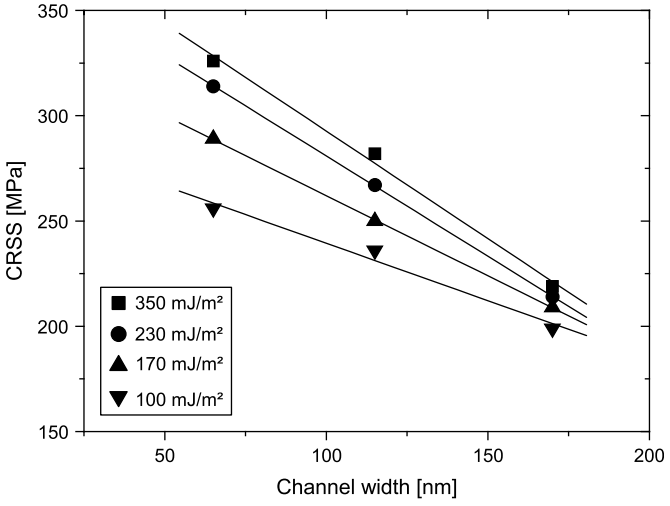

Fig. 4. Effect of the width w of the γ channel on the CRSS to move a 60° 1/2⟨110⟩ dislocation pair through a γ/γ' superalloy at different APB energies, and fixed volume fraction $f = 0.73$. The continuous lines represent a fit of a linear size dependence.

Please cite this article in press as: Vattré A, et al., Dislocation dynamics simulations of precipitation hardening in Ni-based superalloys with..., Intermetallics (2009), doi:10.1016/j.intermet.2009.04.007

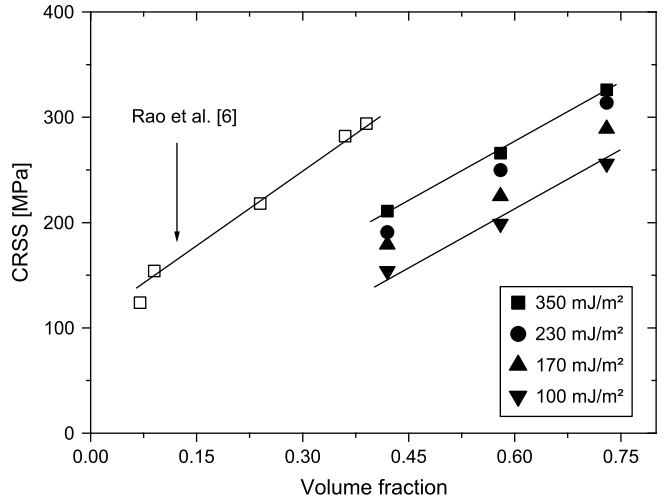

Fig. 5. Effect of the precipitate volume fraction f on the CRSS for different APB energies. In these computations the cutting dislocations form a 60° 1/2⟨110⟩ dislocation pair and the matrix channel width $w = 65$ nm. For comparison, the results of Rao et al. [6] are reproduced. Their simulations were carried out at lower volume fractions and considering a 0.3% coherency strain. Linear fits are plotted as a visual guide.

critical stress required to cut a cubic precipitate as a function of the channel width w and for the two different types of intersections. Here the volume fraction $f = 0.73$ and the APB energy $\gamma^{APB} = 320\ \mathrm{mJ\,m^{-2}}$. For a direct comparison between the two types of intersections, the glide plane in the γ channels is chosen in such a way that the initial segment length in contact with the precipitates is the same in all the simulations.

Fig. 6 shows that in the bowing-assisted cutting regime, the mixed-character dislocation pair requires a higher CRSS for cutting the precipitate than the screw dislocations. This non-intuitive result has already been discussed by Mohles [5] and is explained as follows. The superdislocations needed to cut γ′ precipitates are the most easily formed with a pair of screw dislocations: as a result of elastic interactions at a given stress amplitude, the spacing between two repulsive dislocations pushed against an obstacle attains a minimum for screw dislocations. This explains why for screw dislocations, the formation of superdislocations inside γ′ precipitates occurs at a lower applied stress.

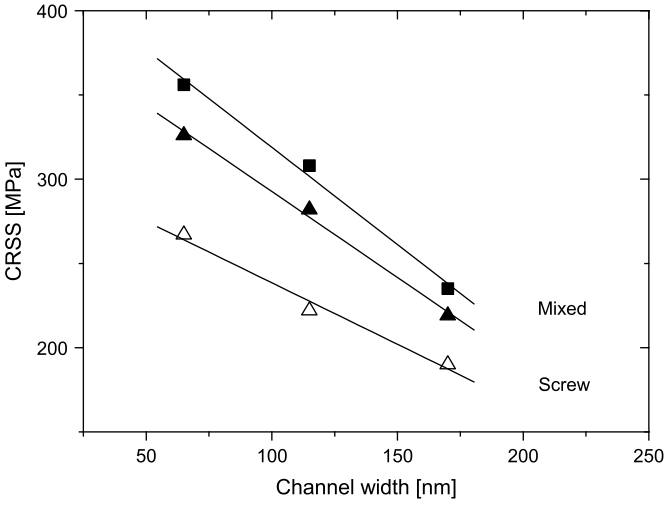

Fig. 6. Critical resolved shear stresses as a function of channel width w for a 1/2⟨110⟩ screw dislocation pair (open symbols) and a 60° mixed dislocation pair (full symbols). In the mixed dislocations case two different precipitate–glide plane intersections are tested. The triangles and squares denote respectively the triangular and irregular hexagonal intersections. The precipitate volume fraction $f = 0.73$.

For all cases, the CRSS decreases quasi-linearly with the channel width w. In addition, it is shown in Fig. 6 that the CRSS obtained with triangular intersections are significantly lower than the corresponding ones calculated with the irregular hexagonal intersections. This difference is simply explained with geometrical arguments. In the hexagonal case, the angle between channels around each corner of the precipitates is 120°, whereas in the triangular case this is 60°. In the latter case, the dislocation pressed against the edges of a precipitate adopts a strong local curvature which intensifies the line tension and elastic self-interactions. The hexagonal and triangular intersections are the two limiting cases which can be calculated with a fixed length of dislocation pressed against a precipitate. The error bars plotted in Fig. 8 account for this geometrical dispersion.

3.5. Influence of the solid-solution friction stress in the γ matrix

In the simulations described so far, the friction stress in the γ matrix τ_{SS} was 107 MPa [9], accounting for the solid-solution hardening there. Fig. 7 shows the influence of this mechanism on the CRSS of the γ/γ′ superalloy, for a channel width $w = 65$ nm, a volume fraction $f = 0.73$, and APB energy $\gamma^{APB} = 320\ \mathrm{mJ\,m^{-2}}$. The increment of the CRSS is found to be approximately the same as the increment of the friction stress: the CRSS increases linearly with increasing frictional stress. Hence, a reduction of dislocation mobility in the γ channels directly affects the mechanical response. This indicates that solid-solution hardening of the matrix is a potent strengthener of γ/γ′ superalloys. In the following section, more attention will be paid to the role of τ_{SS} and its consequences on the overall mechanical response.

3.6. Temperature dependence of the CRSS

The aim of this subsection is to set the simulation parameters in order to reproduce the mechanical behavior of an industrial superalloy with high precipitate volume fraction, and to predict the dependence of the CRSS as a function of temperature. In the following computations a temperature dependence of elastic constants is taken which is based on experimental measurements [22]. According to Parthasarathy et al. [23], the γ^{APB} depends on temperature approximately as $\gamma^{APB} = 320\exp(-((T-297)/2000))$

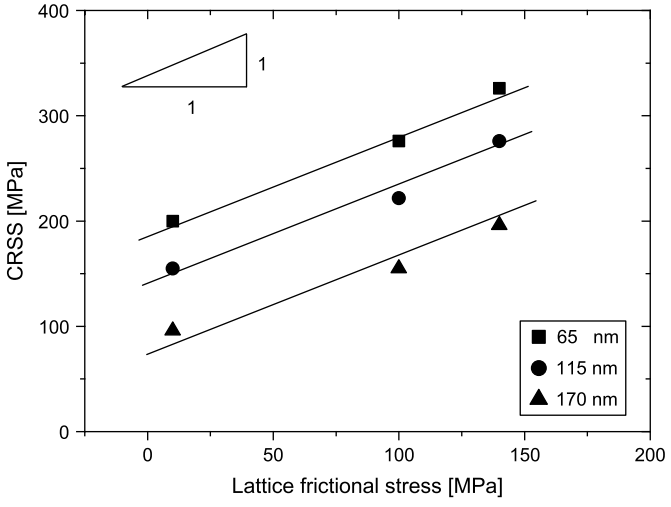

Fig. 7. Effect of solid-solution friction in the γ matrix on the CRSS required to move a 60° 1/2⟨110⟩ dislocation pair at different channel widths w. The continuous lines represent a linear fit of the dependence on the lattice friction.

Please cite this article in press as: Vattré A, et al., Dislocation dynamics simulations of precipitation hardening in Ni-based superalloys with..., Intermetallics (2009), doi:10.1016/j.intermet.2009.04.007

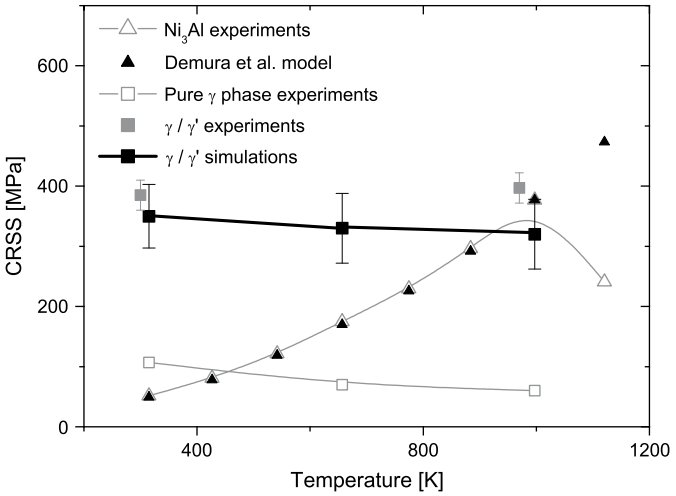

Fig. 8. Simulations of the CRSS for a γ/γ' superalloy as function of temperature (filled black squares) and comparison with experiments [26] (filled grey squares). For comparison the CRSS for Ni_3Al (open triangles for experiments [25] and filled triangles for the Demura et al. model [16]) and Ni solid solution [24] are reproduced. For these simulations $f = 0.73$, $w = 65$ nm, and γ^{APB} as explained in the text.

where $\gamma^{APB} = 320\ mJ\,m^{-2}$ at 297 K [10]. Moreover, a temperature dependence of τ_{SS} was also taken into account. This dependence is fitted from the experimental data summarized by Clément et al. [24]. As reproduced in Fig. 8, τ_{SS} decreases with increasing temperature from about 100 MPa at room temperature to 60 MPa at 1000 K.

In Fig. 8, the simulated CRSS of a two-phase order-strengthened superalloy with a precipitate volume fraction $f = 0.73$ and a channel width $w = 65$ nm is plotted. The simulation results are shown for temperatures up to 1000 K together with the corresponding CRSS of the two constituent phases. The error bars on the simulation results account for the statistical dispersion observed during the calculations. This dispersion is entirely associated to the geometry of the intersection between the glide plane and the precipitate and to the character of the dislocations pairs, as discussed in Section 3.4.

In good agreement with experiments, it is found that the CRSS of the simulated γ/γ' superalloy depends only weakly on temperature up to the maximum tested temperature. As expected, the CRSS reproduced at low temperature is much higher than the corresponding CRSS for each constitutive phase. Moreover, the simulation results are in good quantitative agreement with the response of the industrial single crystal Nickel-based superalloy CMSX-2 containing a volume fraction of γ' precipitates of about 70% [26].

4. Discussion and concluding remarks

Dislocation dynamics simulations have been carried out in order to study the plastic deformation of γ/γ' superalloys with a high volume fraction of γ' precipitates. These simulations account for the most important mechanisms controlling dislocation glide in the two constitutive phases. From a large number of simulations for γ' volume fractions between 0.42 and 0.73 of Ni_3Al precipitates, it is observed that:

- At a fixed precipitate volume fraction $f = 0.73$ and γ channel width $w = 65$ nm, the CRSS of γ/γ' superalloy shows a square root dependence on the APB energy of the γ' phase.
- At a constant γ' volume fraction $f = 0.73$, the CRSS increases linearly with decreasing channel width w, in the range from 65 to 170 nm.
- At a constant channel width $w = 65$ nm, the CRSS increases rapidly with increasing volume fraction of γ' precipitates. This result is consistent with previous simulations carried out at lower volume fractions [6].
- A dislocation pair on a glide plane cutting a precipitate with an irregular hexagonal shape requires a 20% higher resolved shear stress to shear the precipitate than on the alternative triangular intersection, for the same segment length in contact with the precipitate initially.
- For penetrating into a cuboidal precipitate, dislocations initially having a 60° character require a 25% higher resolved shear stress than dislocations with an initial screw orientation.
- Increasing the friction stress τ_{SS} associated to solid-solution elements in the matrix affects directly the CRSS since it decreases the mobility of the dislocations which are bowing out into the γ channels and which are pulling the super-dislocations through the γ' precipitates.

In all the simulated conditions, it can be observed that a pair of dislocations, possibly emitted from the same source, can progress through the microstructure by shearing the γ' precipitates. A strong gliding correlation between pairs of dislocations is observed in the matrix channels. This correlation facilitates the formation of superdislocations and the subsequent process of precipitate cutting. The latter phenomenon is clearly assisted by the dislocations bowing out in the γ channels. As a result of this mechanism, the CRSS measured in the simulations are strongly dependent on the density of solute elements in the γ phase and on the width of the matrix channels. Moreover, the simulated CRSS is found to be weakly dependent on the value of the APB energy in the γ' phase (when considering realistic values larger than $100\ mJ\,m^{-2}$). The latter parameter is nevertheless an essential quantity since it controls the formation of superdislocations when entering precipitates. Incidentally, and in agreement with previous studies carried out at lower precipitate volume fractions, it can be observed that the CRSS required for cutting the γ' precipitates depends on the dislocation character: it is lowest for a pair of screw dislocations because such a dislocation can enter precipitates more easily than other orientations.

The general problem of one pair of infinite dislocations cutting through a periodic microstructure of γ' precipitates is considered in this paper as a critical benchmark test. Such calculations are needed to validate the simulation and to provide a first estimation of the temperature dependence of the CRSS of superalloys with volume fractions larger than 50%. More complex computations are of course needed to account for strain hardening and the orientation dependence on the tensile axis, as observed experimentally. This problem will be discussed in a forthcoming paper accounting for more realistic 3D microstructures. Indeed, multislip simulations are needed to investigate in detail the mechanisms explaining the formation of dislocation pairs, the dislocation–dislocation forest hardening in the γ channels and the accumulation of dislocations at γ/γ' interfaces, which are relaxing strain incompatibilities. The latter feature, as well as the temperature dependence of the misfit stresses in the microstructure of superalloys cannot be simply reproduced by DD simulations, which are usually carried out in periodic cells. A multi-code approach is then needed, for instance a coupling of DD simulations with a finite-element code to solve complex boundary value problems. Such simulations are currently in progress.

Acknowledgements

The authors are grateful to P. Caron (ONERA) and D. Dimiduk (AFRL) for comments and stimulating discussions.

Please cite this article in press as: Vattré A, et al., Dislocation dynamics simulations of precipitation hardening in Ni-based superalloys with..., Intermetallics (2009), doi:10.1016/j.intermet.2009.04.007

References

[1] Kear BH, Wilsdorf HGF. Trans TMS-AIME 1962;224:382.
[2] Westbrook JH. Intermetallic compounds. New York: John Wiley; 1967.
[3] Mohles V, Ronnpagel D, Nembach E. Comput Mater Sci 1999;16(1–4):144–50.
[4] Mohles V. Mater Sci Eng A 2001;319–321:201–5.
[5] Mohles V. Mater Sci Eng A 2004;365(1–2):144–50.
[6] Rao SI, Parthasarathy TA, Dimiduk DM, Hazzledine PM. Philos Mag 2004;84(30):3195–215.
[7] Rao SI, Parthasarathy TA, Dimiduk DM, Hazzledine PM. Philos Mag Lett 2006;86(4):215–25.
[8] Pollock TM, Argon AR. Acta Metall Mater 1992;40:1–30.
[9] Saada G, Douin J. Philos Mag 2004;84(8):807–24.
[10] Veyssière P, Saada G. Microscopy and plasticity of the L12 γ′ phase. In: Dislocations in solids, vol. 10; 1997. p. 253.
[11] Pope DP, Ezz SS. Int Metall Rev 1984;29:136.
[12] Thornton PH, Davies RG, Johnson TL. Metall Trans A 1970;1:207.
[13] Takeuchi S, Kuramoto E. J Phys Soc Jpn 1971;31:1282.
[14] Takeuchi S, Kuramoto E. Acta Metall 1973;21:415.
[15] Paidar V, Pope DP, Vitek V. Acta Metall 1984;435.
[16] Demura M, Golberg D, Hirano T. Intermetallics 2007;15(10):1322–31.
[17] Devincre B, Veyssière P, Kubin LP, Saada G. Philos Mag A 1997;75:1263.
[18] Devincre B, Veyssière P, Saada G. Philos Mag A 1999;79:1609.
[19] Devincre B, Kubin L, Lemarchand C, Madec R. Mater Sci Eng A 2001;309–310:211–9.
[20] Reppich B. In: Mughrabi H, editor. Materials science and technology, vol. 6. New York, Basel, Cambridge: VCH-Weinheim; 1993. p. 321.
[21] Nembach E. Prog Mater Sci Forum 2000;45:275–338.
[22] Unpublished data.
[23] Parthasarathy TA, Rao SI, Dimiduk DM. A fast spreadsheet model for the yield strength of superalloys, Superalloys 2004. TMS (The Minerals, Metals & Materials Society); 2004.
[24] Clément N, Coujou A, Jouiad M, Caron P, Kirchner HOK, Khan T. Superalloys 1996:239–48.
[25] Miura S, Ochiai S, Oya Y, Mishima Y, Suzuki T. In: Liu CT, Taub AI, Stoloff NS, Koch CC, editors. High temperature ordered intermetallic alloys III. MRS symposium proceedings, vol. 133. Pittsburgh: Materials Research Society; 1989. p. 241.
[26] Caron P, Khan T. Advanced materials and processing techniques for structural applications. In: Khan T, Lasalmonie A, ONERA internal report; 1987. p. 59.

Please cite this article in press as: Vattré A, et al., Dislocation dynamics simulations of precipitation hardening in Ni-based superalloys with..., Intermetallics (2009), doi:10.1016/j.intermet.2009.04.007